Restrained Torsional Dynamics of Nuclear DNA in Living Proliferative Mammalian Cells

Marc Tramier,* Klaus Kemnitz,† Christiane Durieux,* Jacques Coppey,* Patrick Denjean,‡ Robert B. Pansu,‡ and Maïté Coppey-Moisan*

*Institut Jacques Monod, UMR 7592, CNRS, Universités P 6/P 7, 75251 Paris cedex 05, France, †EuroPhoton GmbH, D-12247 Berlin, Germany, and ‡Laboratoire de Photophysique et Photochimie Macromoléculaire et Supramoléculaire, Département de Chimie/UMR 85 31, ENS de Cachan/CNRS, 94235 Cachan Cedex, France

ABSTRACT Physical parameters, describing the state of chromatinized DNA in living mammalian cells, were revealed by in situ fluorescence dynamic properties of ethidium in its free and intercalated states. The lifetimes and anisotropy decays of this cationic chromophore were measured within the nuclear domain, by using the ultra-sensitive time-correlated single-photon counting technique, confocal microscopy, and ultra-low probe concentrations. We found that, in living cells: 1) free ethidium molecules equilibrate between extracellular milieu and nucleus, demonstrating that the cation is naturally transported into the nucleus; 2) the intercalation of ethidium into chromatinized DNA is strongly inhibited, with relaxation of the inhibition after mild (digitonin) cell treatment; 3) intercalation sites are likely to be located in chromatin DNA; and 4) the fluorescence anisotropy relaxation of intercalated molecules is very slow. The combination of fluorescence kinetic and fluorescence anisotropy dynamics indicates that the torsional dynamics of nuclear DNA is highly restrained in living cells.

INTRODUCTION

Chromatinized DNA in the nucleus of mammalian cells is highly compacted, forming a basic motif: the nucleosome consists of 1.75 turns of a left-handed superhelix of B-DNA (146 bp of right-handed double helix), folded around an octamer of histones, the core histones. Refined x-ray structural studies show that, at the octamer surface, positively charged aminoacid residues are distributed, according to a path that perfectly fits that of negatively charged phosphate residues of B-DNA (Arents and Moudrianakis, 1993). This tight structure of the nucleosome core particle was confirmed and further refined (Luger et al., 1997). The linker DNA between nucleosomes is typically associated either with histone H1/H5 to promote a more dense packaging (for recent paper see Leuba and al., 1998) or with multiprotein complexes involved in DNA transactions (see, for review on replication, Baker and Bell., 1998; on transcription, Carey, 1998; Ashraf and Ip, 1998). Packaging DNA into chromatin inhibits the progressions of RNA and DNA polymerases in vitro (reviewed in Owen-Hughes and Workman, 1994; Widom, 1998), but nevertheless, the cell replicates and transcribes DNA in vivo. In recent models, derived from in vitro analysis of polymerization over nucleosomal templates, the existence of naked DNA regions was supposed to occur transiently and over short segments (which can be as small as 10 bp), due to partial or full dissociation of histone octamer from the DNA (Studitsky et al., 1997).

Some experiments tried to determine the chromatin structure within the whole cell: size of linker DNA (review by van Holde, 1989), degree of supercoiling of linker regions (Jupe et al., 1993), higher-order organization (Rydberg et al., 1998), rotational reorientation (Selvin et al., 1990), and dynamics (reviewed by Lamond and Earnshaw, 1998; Manders et al., 1999) of chromatin. In most experiments, however, cells were either fixed or permeabilized, or detection was carried out on extracted chromatin. Protein–DNA interactions, involved in native chromatin structure, can be easily perturbed during cell manipulation or observation, as it had been shown to occur, when illuminating living cells labeled with fluorescent dye, at standard low-light levels that were still not low enough to avoid photodynamic reaction (Delic et al., 1991). Thus, the organization of chromatin in vivo can be considered to be still largely unknown, partially due to invasive techniques that were so far applied.

The fact that nuclear DNA replicates over the full length in vivo, and this within a few hours of each cell cycle, suggests that, inside cells, nuclear DNA (which is under nucleosomal arrangement, when extracted) would interact with chromosomal proteins in a dynamic way, revealing to some extent intrinsic properties of the double helix, such as elasticity and flexibility, to allow the progression of the polymerases over the nucleosomal template. Our goal was, therefore, to examine whether nuclear DNA in living cells is endowed with structural dynamics. Twisting rigidity of DNA is an important determinant of the energetics of formation of complicated nucleoprotein structure (Echols, 1986). The interaction of some proteins, such as High Mobility Group I, requires bending and untwisting of DNA, modifying the minor groove to fit to the contour of the protein (Grosschedl, 1995). Fluorescence anisotropy decay studies of the ethidium-DNA complex were performed to investigate internal motion of DNA (Wahl et al., 1970). The

Received for publication 1 November 1999 and in final form 31 January 2000.

Address reprint requests to Dr. Maite Coppey-Moisan, Macromolecular Complexes in Living Cells, Institut Jacques Monod, UMR 7592 P6/P7, 2 Place Jussieu-Tour 43, 75251 Paris cedex 05, France. Tel.: +33-1-44-27-79-51; Fax: +33-1-44-27-79-51; E-mail: coppey@ijm.jussieu.fr.

© 2000 by the Biophysical Society

0006-3495/00/05/2614/14 $2.00

experimental fluorescence depolarization was theoretically analyzed in the frame of twisting motions of the DNA along the helix axis. These models are particularly appropriate to investigate the torsional dynamics of DNA (Allison and Schurr, 1979; Schurr, 1984) and the restriction of these dynamics upon structural deformation by bending strain (Heath et al., 1996) or by tight immobilization of both DNA chains in nucleosome core particle (Winzeler and Small, 1991).

Ethidium does, indeed, enter living cells, as had been shown earlier (Delic et al., 1992; Hayashi et al., 1994; Coppey-Moisan et al., 1996; Favard et al., 1997), but even with intensified fluorescence digital imaging microscopy, it was not possible to detect intercalation in nuclear DNA of living proliferative mammalian cells (Delic et al., 1991, 1992; Coppey-Moisan et al., 1996). Fluorescence lifetime measurement under the microscope (Minami and Hirayama, 1990; Verkman et al., 1991; Buurman et al., 1992; Lakowicz et al., 1992; Piston et al., 1992; Morgan et al., 1992; French et al., 1992; Gadella et al., 1993; Ambroz et al., 1994; So et al., 1995), recently became an emerging technology for quantitative imaging in living cells (Bastiaens and Squire, 1999; Dayel et al., 1999). By taking advantage of the different fluorescence lifetimes of ethidium in the bound and free states (Olmsted and Kearns, 1977) and of the very sensitive detection method of time-correlated single photon counting, combined with confocal microscopy (Nakatani et al., 1993; Schoutteten et al., 1997), extremely low fluorescence from intercalated ethidium molecules could be detected in the nucleus of living mammalian cells. In addition, fluorescence anisotropy decay dynamics allowed us to show that the native cellular state is characterized by restrained torsional motion of nuclear DNA and by a strong inhibition of ethidium intercalation in nuclear DNA.

MATERIALS AND METHODS

Chemicals

Rhodamine 6G chloride, ethidium bromide, and Hoechst 33342 were from Molecular Probes Europe (Leiden, The Netherlands), digitonin was from Sigma (St Quentin Fallavier, France), 1-butanol from Aldrich (St Quentin Fallavier, France), and λ-DNA was purchased from Pharmacia Biotech Europe (Orsay, France).

Cell culture and labeling with ethidium

S2 cells, a clonal expansion from a transformed Vero monkey kidney cell line (Gao and Knipe, 1989), were grown in Dulbecco's modified minimal essential medium (Gibco, Cergy-Pontoise, France), supplemented with 10% fetal calf serum. The experiments were carried out at a relatively low density of S2 cells, i.e., after 48–72 h of a culture of 3×10^5 cells, seeded on 12.5 cm^2 round glass coverslip (H. Saur, Reutlingen, Germany). Cells were incubated with 0.1–10 μg/ml ethidium bromide in growth medium for 30 min at 37°C. For experiments under the microscope, the coverslip was mounted in an open observation chamber (H. Saur) and the cell monolayer was rinsed with 20 mM Hepes-buffered Hank's balanced salt solution, which contained ethidium bromide at the same concentration as that used in incubation experiments, for measurements done in the presence of ethidium bromide.

For permeabilization experiments, cells were preloaded with a mixture of 1 μg/ml Hoechst 33342 and 4 μg/ml ethidium bromide for 30 min at 37°C. Permeabilization treatment was carried out by adding 50 μg/ml of digitonin to the observation medium, Hepes-buffered Hank's balanced salt solution, at room temperature.

For naked DNA measurements, a solution of λ-DNA (50 μg/ml) and ethidium bromide (0.5 or 4 μg/ml) in water was used. The ratio of dye/basepair was 1/15 for lifetime measurements and was kept below 1/150 for anisotropy acquisition to avoid energy transfer.

Fluorescence microscopy imaging at low light level

Epi-fluorescence imaging was carried out at room temperature on living or permeabilized cells, using an inverted microscope DMIRBE (Leica, Rueil-Malmaison, France). Fluorescence images were acquired at very low excitation light levels as described elsewhere (Delic et al., 1991) with some modifications. Briefly, cells grown on glass coverslips were mounted in an open observation chamber and imaged through an ultrafluor objective (100× magnification, NA = 1.3). The detector was a cooled, slow-scan CCD camera with 1024 × 1024 pixels, digitized on 4096 grey-levels (SILAR, St. Petersburg, Russia). The excitation source was a 50 W high-pressure mercury lamp. For ethidium fluorescence, we used λ_{exc} = 540 nm, OD = 2, and $\lambda_{em} > 590$ nm, and, for Hoechst 33342, λ_{exc} = 365 nm, OD = 2, and 480 nm $< \lambda_{em} <$ 520 nm. Background subtraction, shading correction, and other image processing were carried out as described elsewhere (Coppey-Moisan et al., 1994), by using Khoros software (Khoral Research, Albuquerque, NM USA).

Fluorescence lifetime measurements and data analysis

The confocal microscope, used for acquisition of fluorescence decay dynamics, is described elsewhere (Schoutteten et al., 1997). Briefly, a titanium: sapphire picosecond laser (Spectra Physics France, Les Ulis, France), λ_{exc} = 498 nm, 4 MHz, was directed through the light-inlet port of a Nikon epi-fluorescence inverted microscope. Subcellular localization of the excitation volume was selected by observing the diffracted laser spot simultaneously with the transmitted white light cell image. The depth within the nucleus was adjusted by using a piezoelectric displacement of the objective (Polytec-PI, Pantin, France). The fluorescence photons, emitted from the illuminated volume of 1 μm^3, were collected by a 100× magnification objective (NA = 0.8–1.3) and conducted through an optic fiber (400 μm) to a time-correlated single photon counting system with a microchannel plate-photomultiplicator tube detector R3809U (Hamamatsu Photonics France, Massy, France). Scattered excitation light was removed by a glass cut-off filter, inserted in front of the detector. The standard time-correlated single photon counting system (O'Connor and Phillips, 1984) was operated at 2048 channels, using time windows from 50 to 200 ns. A Fresnel rotator was placed in the excitation laser beam and a sheet polarizer before the optical fiber on the emission path. Vertical (v) and horizontal (h) positions of the excitation and emission polarizations, abbreviated as vv, hv, hh, vh, were obtained by rotating the Fresnel rotator and the sheet polarizer. Two fluorescent decays were acquired, parallel ($i_{vh}(t)$) and perpendicularly polarized ($i_{hh}(t)$). A third decay was acquired at the magic angle, with the Fresnel rotator positioned 55° away from the vertical direction and the polarizer oriented in the horizontal direction. Small deviations from the magic angle, caused by slight polarization at the dichroic mirror, had no influence on extracted lifetimes and the preexponential factors, which were in agreement with that recovered from the fluorescence decay acquired with the Fresnel rotator positioned at the magic angle, $i_{mag}(t)$, and from the total fluorescence, $i(t) = i_{vh}(t) + 2i_{hh}(t)$.

The same count rate was used for acquisition of fluorescence and instrument response function (IRF), which was measured by focusing the laser on the surface of a microscope glass slide and by taking off the cut-off filter.

Global analysis software was Globals Unlimited (Illinois University). It allowed application and investigation of divers kinetic models, such as decay-associated anisotropy, and performance of rigorous error analysis and simulations. Static background, as measured by the mean number of counts before the rise of fluorescence, was treated as a fit parameter by the kinetic analysis software. Dynamic background was acquired from a background sample (e.g., medium) under identical conditions and incorporated in the analysis. Fluorescence decays were deconvoluted with the IRF and fitted by a Marquardt nonlinear least-square algorithm. When modeling anisotropy decays, a *g*-factor was used as free or fixed fit parameter. Global analysis was performed for parallel and perpendicular decays.

Measurement of intracellular concentration of ethidium

The concentrations of free and intercalated nuclear ethidium were calculated from measurements of the fluorescence decays in the nucleus and in the extracellular medium, in the presence of a given ethidium concentration in the incubation medium. Two magic angle decays were measured with the same acquisition time (200 s), the laser being focused in the extracellular medium and then in the nucleus, and fitted with fixed typical lifetimes for free (τ_{free} = 1.8 ns) and intercalated (τ_{int} = 22 ns) ethidium. The pre-exponential factors were determined by the best global fit of the model functions

$$i_{ext}(t) = a_0 e^{-t/\tau_{free}} \quad (1)$$

$$i_{nuc}(t) = a_{free} e^{-t/\tau_{free}} + a_{int} e^{-t/\tau_{int}}, \quad (2)$$

where a_0 is the pre-exponential factor corresponding to free ethidium in the extracellular medium, and a_{free} and a_{int}, are those corresponding to free and intercalated ethidium in the nucleus, respectively.

For each fluorescence decay, the relation between concentration, C, and pre-exponential factor, a, is

$$a = K\varepsilon C k_r, \quad (3)$$

where ε is the absorption coefficient, k_r the radiative rate constant, and K a factor that depends on experimental parameters (sampling volume, laser power, and acquisition time).

Assuming that: the experimental variations were negligible during an experiment (K = const), the free ethidium lifetimes are identical in extracellular medium and in the nucleus, and the radiative rate constant is identical for free and intercalated ethidium species, as had been claimed earlier (Olmsted and Kearns, 1977), we obtain the ratios

$$a_0/a_{free} = C_0/C_{free} \quad \text{and} \quad a_{free}/a_{int} = \varepsilon_{free} C_{free}/\varepsilon_{int} C_{int}, \quad (4)$$

where $\varepsilon_{free}/\varepsilon_{int}$ = 1.456 at 498 nm excitation.

C_{free} and C_{int} were calculated then for each known C_0 concentration of ethidium at the end of the incubation period.

Measurements of fluorescence anisotropy decay

Anisotropy measurements were carried out using the same set-up as that for lifetime measurements (Schoutteten et al., 1997). The optical design of the microscope results in four geometric components of the fluorescence polarization, where i_{vh} and i_{hv} pertain to the parallel direction and i_w and i_{hh} to the perpendicular direction, with the first index standing for excitation and the second for emission.

The decays $i_{vh}(t)$ and $i_{hh}(t)$ were chosen as parallel and perpendicularly polarized fluorescence decays, respectively, and were acquired sequentially. To correct for different transmission efficiency of each geometric component of the excited and emitted polarized light, as well as for polarizing (or depolarizing) effects of the microscope optics, a G factor was experimentally determined by acquiring the four geometric components with steady-state illumination (i_{vh}, i_{hh}, i_{hv}, i_{vv}).

$$G = [(i_{vh} \times i_{vv})/(i_{hv} \times i_{hh})]^{1/2} \quad \text{(see Eq. A10).} \quad (5)$$

In addition, a normalization factor, T, was determined by experiment to correct for laser fluctuations, acquisition times, and potential photobleaching:

$$T = i_{vh} \times \int i_{hh}(t)\, dt / i_{hh} \times \int i_{vh}(t)\, dt \quad \text{(see Eq. A4).} \quad (6)$$

$\int i_{hh}(t)\, dt$ and $\int i_{vh}(t)\, dt$ are the total intensity of the perpendicular and parallel polarized fluorescence, respectively, integrated over the acquisition time and measured from the surface areas under the $i_{hh}(t)$ and $i_{vh}(t)$ curves of a 200 ns time window.

The anisotropy function, $r(t)$, was calculated (without deconvoluting the instrument response function) from

$$r(t) = \frac{T\, i_{vh}(t) - G\, i_{hh}(t)}{T\, i_{vh}(t) + 2\, G\, i_{hh}(t)} \quad \text{(see Eq. A13).} \quad (7)$$

To validate this normalization method of the parallel and perpendicular decays, the rotational behavior of rhodamine 6G in butanol, taken as a reference, was measured in two independent ways: the classic "tail matching" method (Appendix B), and by measuring the normalization factor T and the geometric correction factor G, as described above and in Appendix A.

For small, freely rotating molecules such as rhodamine 6G in low-viscosity solvents such as butanol, the parallel and perpendicular polarized decays can be fitted with the model functions,

$$i_{vh}(t) = \mathrm{IRF}(t) * [ae^{-t/\tau} \times (1 + 2r_0 e^{-t/\phi})], \quad (8)$$

$$i_{hh}(t) = g \times \mathrm{IRF}(t) * [ae^{-t/\tau} \times (1 - r_0 e^{-t/\phi})] \quad \text{(see Eq. B12 and B13),} \quad (9)$$

with IRF(t) being the instrument response function, τ the fluorescence lifetime, r_0 the anisotropy at time zero, and ϕ the rotational time of rhodamine 6G in butanol. g is a factor to correct for the different transmission efficiency of the two experimental decays, $i_{vh}(t)$ and $i_{hh}(t)$.

In the first case, the parameters of fluorescence and rotational kinetics (τ, r_0, and ϕ) were directly found from the best fit of both Eqs. 8 and 9, leaving g as a fit parameter and assuming that the anisotropy is zero at long time (tail matching method).

In the second case, $i_{vh}(t)$ and $i_{hh}(t)$ were normalized before the fit in $i_{par}(t)$ and $i_{per}(t)$, respectively, with the expressions,

$$i_{par}(t) = T \times i_{vh}(t) \quad (10)$$

and

$$i_{per}(t) = G \times i_{hh}(t), \quad (11)$$

which were derived from Eq. A13. In this case, the g coefficient was set to 1 and the parameters of the fluorescence and rotational kinetics (τ, r_0, and ϕ) were recovered from the best fit of the functions,

$$i_{par}(t) = \mathrm{IRF}(t) * [ae^{-t/\tau} \times (1 + 2r_0 e^{-t/\phi})], \quad (12)$$

$$i_{per}(t) = \mathrm{IRF}(t) * [ae^{-t/\tau} \times (1 - r_0 e^{-t/\phi})]. \quad (13)$$

In general, both methods yielded identical results (see Results).

To avoid photodynamic reaction, especially during measurements in living cells, neutral density filters were placed in the laser beam to obtain a laser average energy of a few nano-Watts only at the entrance of the microscope. All cellular measurements were carried out using NA = 1.3 to have the best collection efficiency of fluorescence light.

Simulation of anisotropy decays of ethidium fluorescence

Simulations of anisotropy relaxation were based on various models, such as decay-associated rotation times (Beechem et al., 1991) with two emitting species of the same concentration, one with a short lifetime (1.8 ns) and a short anisotropy relaxation time (250 ps), the other with a long lifetime (22 ns) and a long anisotropy relaxation time (250 ns). These lifetime values are modeling free and intercalated ethidium. The simulations used a specific kinetics model, such as the above, an experimental IRF, and added Poisson noise, to obtain idealized experimental decays for horizontal and vertical polarizations. Reanalysis of the simulated decays yielded the original kinetic parameters of the model, thus confirming the integrity of the fitting procedure. Phenomenological decay parameters obtained by the above method, however, do not necessarily describe the relevant biological situation.

Schurr and coworkers addressed this situation by modeling DNA as a series of rigid rods, connected by torsion springs at their joints, each rod corresponding to one basepair, thus developing a theoretical expression for fluorescence anisotropy decay of ethidium intercalated in DNA (Allison and Schurr, 1979). This early model neglects rapid restricted dye wobbling, DNA bending motions, and global motions of the whole DNA. Simulations of the experimental fluorescence anisotropy decay of ethidium, intercalated in λ-phage DNA solution and in the nucleus of living cells, were carried out by using a simplified expression corresponding to the "intermediate zone formula" of the model (Thomas et al., 1980). An advanced model takes into account protein–DNA interactions, consisting of a finite filament rigidly clamped at both ends (Schurr, 1984; Schurr and Schurr, 1985). These models yield the following expression for the fluorescence anisotropy decay of ethidium, rigidly bound to either naked or chromatinized DNA:

$$r(t) = r_0[(3/2\cos^2\varepsilon_0 - 1/2)^2 + 3\cos^2\varepsilon_0\sin^2\varepsilon_0 C_1(t) + 3/4\sin^4\varepsilon_0 C_2(t)], \quad (14)$$

where $\varepsilon_0 = 70.5°$, the angle between the transition dipole and the helix axis (Schurr and Schurr, 1985), $C_1(t)$ and $C_2(t)$ are the correlation functions $C_n(t)$, for $n = 1$ and $n = 2$, which model torsional motions of DNA:

$$C_n(t) = \exp[-n^2 k_B T(t/\pi\alpha\gamma)^{1/2}] \quad (15)$$

for long linear DNA corresponding to infinite rigid rods, and

$$C_n(t) = 1/N \sum_{m=1}^{N} \exp\left\{-n^2 \sum_{l=1}^{N} d_l^2 Q_{ml}^2[1 - \exp(-t/\tau_l)]\right\} \quad (16)$$

for finite DNA rigidly clamped at both ends, with

$$Q_{ml} = [2/(N+1)]^{1/2}\sin[ml\pi/(N+1)], \quad (17)$$

$$d_l^2 = (k_B T/\gamma)\tau_l, \quad (18)$$

$$\tau_l = \gamma/\{4\alpha\sin^2[l\pi/2(N+1)]\}, \quad (19)$$

where k_B is the Boltzmann's constant and T the absolute temperature. The anisotropy behavior is characterized by three parameters, α, γ, and N. The twisting correlation functions are dependent on α, the torsional spring constant describing the properties of the torsional spring between the rigid rods, γ, the frictional factor of the rigid rods proportional to viscosity of the medium, and N the number of rigid rods between points of attachment (for the second model). Computations of these expressions were made for the time span of 0 to 70 ns, with $r_0 = 0.25$, representative of typical experimental conditions (Igor software).

RESULTS

Fluorescence anisotropy decays under the microscope

Fluorescence anisotropy measurements, under the microscope, of chromophores bound to deformable polymers as DNA, exhibit two types of difficulties: light depolarization or polarization due to the objective and dichroic mirror, and normalization of the parallel and perpendicular intensities. For small molecules in solution, for which the rotational time is short compared to the fluorescence lifetime, this normalization can be carried out by assuming that molecules completely relax, thus that the anisotropy is zero at long times (tail matching method). This normalization cannot be applied to molecules for which the rotational time (or twisting deformations in the case of DNA) is longer than the fluorescence decay time.

Before performing studies on DNA in living cells, these two aspects were first investigated using rhodamine 6G in butanol as standard. Measurements of parallel and perpendicular polarized rhodamine 6G fluorescence decays were performed for two numerical apertures (NA) of the objective. The anisotropy decays were obtained first by the classic way of normalization (tail matching) (Fig. 1). The initial decay zones of the fluorescence anisotropy obtained with two NA were different, because of the different value of anisotropy at time zero (r_0) as shown in Table 1.

A theoretical approach by Axelrod (1979, 1989) describes the decrease of r_0 with increasing the NA of the objective. Our experimental results are in good agreement with the Axelrod's formulae (Fig. 2). Depolarization by the

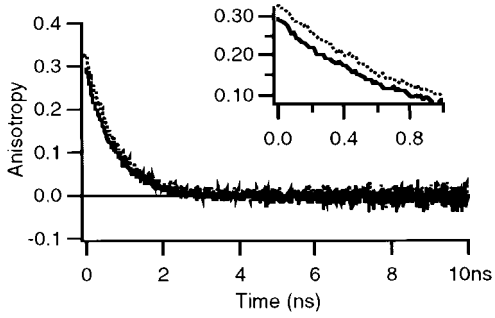

FIGURE 1 Anisotropy decays of rhodamine 6G fluorescence in butanol under the confocal microscope. Fluorescence decays used for the calculation of the anisotropy function were normalized by tail matching. Measurements were made at 1.3 (*solid*) and 1 (*dotted*) numerical aperture of a 100× objective. The fit parameters are presented in Table 1.

TABLE 1 Comparison of rotational parameters of rhodamine 6G obtained by different normalization methods of polarized decays and different NA of the objective

	a*	τ (ns)*	r_0*	ϕ (ps)*
Tail matching normalization				
NA = 1.3	15.4 ± 0.4	3.4 ± 0.1	0.296 ± 0.024	830 ± 120
NA = 1	13.7 ± 0.4	3.4 ± 0.1	0.320 ± 0.022	820 ± 90
Experimental normalization				
NA = 1.3	15.1 ± 0.4	3.4 ± 0.1	0.292 ± 0.036	770 ± 100
NA = 1	12.5 ± 0.4	3.4 ± 0.1	0.320 ± 0.021	800 ± 70

Results of the fitted anisotropy decays of rhodamine 6G in butanol, using the two different normalization methods, Tail matching and experimental normalization with G and T factor (see Material and Methods and Appendix A). Measurements were made at two different numerical apertures of the 100× magnification objective, 1 and 1.3.

*a, pre-exponential factor; τ, fluorescence lifetime; r_0, anisotropy value at time zero; ϕ, rotational time.

optical set-up of the microscope, however, did not change the recovered kinetic parameters for fluorescence decays and fluorescence anisotropy decays. Lifetime and rotational time of rhodamine 6G in butanol, 3.4 ns and 820 ps, respectively, were very similar when measured at two different NA values (Table 1). The dynamics values are consistent with the apparent volume of the molecule and viscosity of the medium in terms of the Perin's equation and agree with literature (Philips et al., 1985).

Because tail matching normalization is impossible for fluorescence anisotropy decay of ethidium intercalated in DNA, a new experimental normalization for time-resolved anisotropy measurement in confocal microscopy was developed (see Materials and Methods and Appendix A). To validate our method, a comparison of this new experimental normalization with standard normalization was performed on rhodamine 6G solutions at two different NA (1 and 1.3). Results for the two normalizations, using the same fluorescent decays, are given in Table 1. The small differences of fit parameters between the two normalization procedures were not significant and were well within the error domain, obtained by rigorous error analysis.

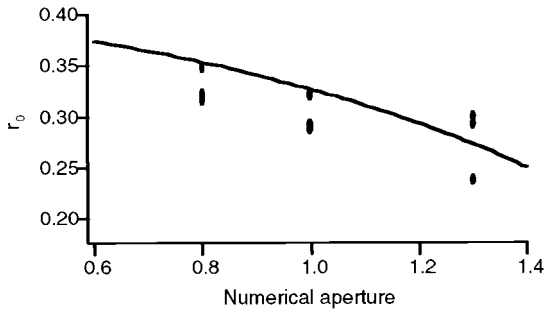

FIGURE 2 Dependence of anisotropy at time zero (r_0) on the numerical aperture of the objective. Experimental data (*symbol*) are shown for Rhodamine 6G in butanol, using a 100× objective. The theoretical curve (*solid*) takes into account differences due to the aperture of the objective in the optical path and the geometric orientation of the polarized light (Axelrod, 1979).

Evidence of ethidium intercalation in the nucleus of living cells

The ethidium fluorescence image of a living proliferative cell, acquired at low level of excitation light, is displayed in Fig. 3 *A*. An extremely low level of excitation intensity is required for photodynamic reaction to be avoided and for the living state to be preserved (Delic et al., 1991). Under these conditions, ethidium enters living cells, intercalates in mitochondrial DNA (Coppey-Moisan et al., 1996) and in double-stranded regions of ribosomal RNA in nucleoli (Delic et al., 1992), but no steady-state fluorescence intensity could be detected so far in the nucleus (nucleolus excepted) (Fig. 3 *A*). The presence of free and intercalated ethidium in the nucleus, however, was established by time-correlated photon counting. This relies on the fact that fluorescence photons only are time-correlated but not the noise, which allows extraction of extremely weak fluorescence signal from the background. Fluorescence decay measurements were carried out in confocal mode on subnuclear regions. The nucleoli were avoided because they were clearly visible in the transmitted cell image. Measurements were done successively in the extracellular medium and in the nucleus (Fig. 3 *B*), on the same cell culture and in the presence of the same extracellular concentration of ethidium (1 μg/ml) than that in Fig. 3 *A*. In the extracellular medium, a short decay time of 1.8 ns, indicative of free ethidium, was obtained. In the nucleus, a bi-exponential decay was observed with lifetimes of 1.8 ns (free ethidium) and 22 ns, where the long lifetime is characteristic of ethidium intercalated in DNA/RNA, and caused by reduced accessibility of ethidium molecules to proton acceptors (Olmsted and Kearns, 1977).

The absolute concentrations of ethidium in the nucleus, free and intercalated, were calculated as described in Materials and Methods. The obtained values are reported in Table 2 for three separate experiments carried out at three ethidium concentrations applied to the extracellular medium. The decays of ethidium fluorescence were fitted by fixing the two lifetimes of 1.8 ns and 22 ns, representative of free and intercalated ethidium, respectively. By using this method, nuclear autofluorescence and fluorescence from ethidium species with an intermediate lifetime (~10 ns) were neglected. Cells without ethidium labeling revealed two dominant lifetimes of 400 ps (80%) and 3.5 ns (20%), corresponding to nuclear autofluorescence and being quite different from ethidium lifetimes. In addition, the contribution of autofluorescence never exceeded 15% of the ethidium fluorescence, even at the lowest ethidium concentration used (data not shown). At longer acquisition times and higher ethidium concentrations, the decay of ethidium could better be fitted by three exponentials, with an addi-

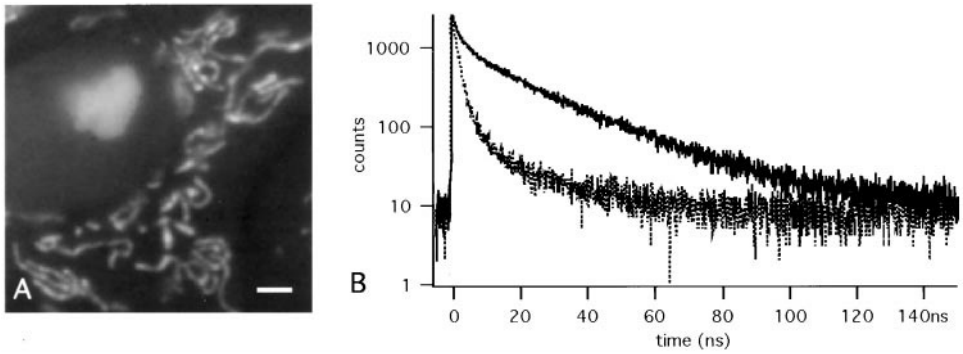

FIGURE 3 Evidence for intercalated ethidium in the chromatin of living S2 cells, in the absence of any steady-state ethidium fluorescence in standard fluorescence imaging microscopy. (*A*) Steady-state ethidium fluorescence image of a living S2 cell, acquired with an intensified camera. Bar, 5 μm. (*B*) Time-resolved fluorescence in confocal microscopy from a small volume (1 μm^3) of the chromatin area (*upper*) and from the same volume of extracellular medium (*lower*). S2 cells were incubated for 30 min in the presence of 1 μg/ml ethidium bromide at 37°C.

tional intermediate lifetime of about 10 ns, as had been observed before with hairpin structures of DNA (Hernandez et al., 1994) and with tRNA in solution (Hazlett et al., 1989). The contribution of this component, however, never exceeded 10% in living cells (Table 3). The neglect of this intermediate component and of autofluorescence might explain the small differences between free ethidium concentrations in the extracellular medium and in the nucleus (Table 2). In spite of the above simplification, however, it is quite clear that the cytoplasmic membrane does not impede ethidium diffusion inside living cells.

The ratio dye molecule/basepair (Dye/bp) was calculated by assuming the nucleus to be a sphere of 10-μm radius and containing an average of 2×10^{10} bp for this type of cell. Double-stranded regions of nuclear RNA (excluding nucleolar RNA) were neglected. Some cells are in the G2 phase of the cycle, because the cells studied here are in the proliferating state. Being unable to discriminate between G1 and G2 cells, the ratio Dye/bp, as presented in Table 2, might be lower by a factor two. Thus, for the lowest ethidium concentration applied, as few as one intercalated ethidium molecule per 10,000 basepairs of nucleic acids could be detected in the nucleus (nucleolus excluded) of living cells. This nicely shows that time-correlated single-photon counting is an exquisitely sensitive, minimally invasive method, well suited for living cell studies.

Inhibition of ethidium intercalation in nuclear DNA

Figure 4 compares the decays of ethidium fluorescence in the nucleus of living proliferating cells at different extracellular ethidium concentrations (0.4, 1, and 10 μg/ml) and in a solution of λ-phage DNA. At least two exponentials are present in the decay curves, obtained from experiments carried out on subnuclear regions in the living cell. In contrast, the kinetics of ethidium fluorescence of the λ-phage DNA sample was mono-exponential. The kinetic fit parameters are presented in Table 3, revealing that the majority of ethidium molecules (about 60%) present in the nucleus of living cells, is in the free, nonintercalated state. Although the ratio of dye/basepair is much higher in the λ-phage DNA sample (Dye/bp ~1/15) than in the nucleus ($1/10^4 <$ Dye/bp $< 1/10^3$) (see Table 2), no free ethidium could be seen (<10%, detection limit) in the solution of naked DNA, with virtually all ethidium molecules being intercalated with a lifetime of 21.3 ns (Table 3). Thus, the

TABLE 2 Quantification of free and intercalated ethidium in the nucleus of a living cell at different extracellular concentrations

C_0 (μg/ml)	a_0	a_{free}	a_{int}	C_{free} (μg/ml)	C_{int} (μg/ml)	Dye/bp Ratio
0.07	0.043 ± 0.004	0.105 ± 0.010	0.023 ± 0.002	0.17 ± 0.04	0.06 ± 0.02	0.0001
0.30	0.168 ± 0.009	0.211 ± 0.014	0.080 ± 0.003	0.38 ± 0.05	0.21 ± 0.06	0.0003
0.67	0.383 ± 0.018	0.274 ± 0.014	0.138 ± 0.004	0.48 ± 0.05	0.35 ± 0.07	0.0005

Decay measurements were carried at the same acquisition time (200 s) and fitted by two components of fixed lifetimes (1.8 and 22 ns).
a_0, and a_{free} are the pre-exponential factors of the obtained fit, corresponding to free ethidium in extracellular medium and in the nucleus, respectively. a_{int} is the pre-exponential factor corresponding to intercalated ethidium in the nucleus. C_0, and C_{free} are the concentrations of free ethidium in the extracellular medium and in the nucleus, respectively. C_{int} is the concentration of intercalated ethidium in the nucleus. The ratio of dye/base pair in the nucleus was estimated by considering the nucleus as a sphere of 10-μm radius, containing an average of 2×10^{10} bp.
The error domains for a_i were obtained by rigorous error analysis. The error domains for C_i were obtained by calculating the extreme values of concentrations by using the extreme values of the error domain of a_i. For calculation of concentration, see Materials and Methods.

TABLE 3 Fit of fluorescence decays for ethidium in a solution of λ-phage DNA and for ethidium in the nucleus of living S2 cells

	a_1	τ_1	a_2	τ_2	a_3	τ_3	χ^2
λ DNA	1	21.3					1.009
Nuclear DNA							
0.4 μg/ml	0.40	22.1			0.60	2.08	1.187
1 μg/ml	0.36	21.0			0.64	1.95	1.481
10 μg/ml	0.20	26.5	0.07	10.8	0.73	1.85	1.218

After deconvolution with the instrument response function, fits of the fluorescence decays of Fig. 4 were obtained with one, two, or three components.

a_1, a_2, and a_3 are the pre-exponential factors of each components (sum of $a_i = 1$) with fluorescence lifetime of τ_1, τ_2, and τ_3. Values of χ^2 indicate the quality of the fit.

high ratio of free/intercalated ethidium in the nucleus, observed over a wide range of ethidium concentrations (0.1–10 μg/ml), clearly reveals a strong inhibition of intercalation in nuclear DNA of these living cells. This result holds true for all types of proliferating mammalian cells so far examined (Hela cells, exponentially growing fibroblast cells).

It could be assumed that the high level of compaction of DNA inside the nucleus, compared to that of DNA in solution, might be the main process involved in the inhibition of intercalation. This possibility could be ruled out, however, because intercalation could be induced, at least in some nuclear regions (evidenced by a high steady-state fluorescence of ethidium in nuclear DNA), by digitonin treatment (Fig. 5 *D*), at constant nuclear volume. The volume of the nucleus, imaged by Hoechst 33342 fluorescence, and thus the global compaction of DNA within the nucleus, was unchanged before (Fig. 5 *A*) and after (Fig. 5 *C*) digitonin treatment. The increase of ethidium intercalation after digitonin treatment (Fig. 5 *D*) cannot be ascribed to higher membrane permeability for ethidium, because ethidium easily enters into living cells without the presence of digitonin (Tables 2 and 3). Furthermore, the pattern of ethidium fluorescence (Fig. 5 *D*) coincides with regions of highly condensed chromatin, close to the nuclear membrane and around nucleoli, visualized with Hoechst 33342 labeling (Fig. 5 *C*). Thus, the strong inhibition of ethidium intercalation, observed in the unperturbed state of the living cell, was not due only to a high level of compaction of DNA. The effect of digitonin on the nucleus is not known. The observed perturbation of chromatin could either be due to a direct effect of digitonin on chromatin, particularly in those regions being in contact with the nuclear membrane, or could represent an indirect effect arising from modification of the nuclear ionic composition. The loss of mitonchondrial ethidium fluorescence after digitonin treatment (Fig. 5 *D*) is in agreement with our previous observations that a decrease of mitochondrial electrochemical gradient triggers the extinction (or the decrease) of fluorescence of ethidium, preintercalated in mitochondrial DNA (Coppey-Moisan et al., 1996; Durieux et al., 1999). In the present

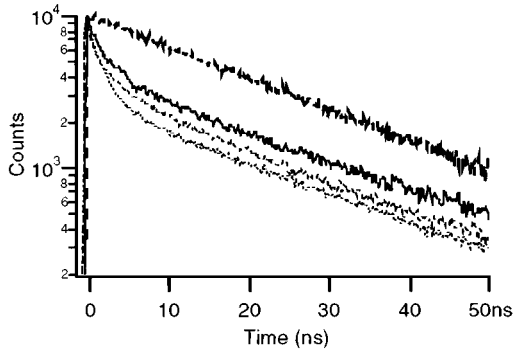

FIGURE 4 Normalized fluorescence decays of ethidium from λ-phage DNA solution and from the nucleus of a living cell. From *top* to *bottom:* λ-phage DNA/ethidium, S2/0.4 μg/ml ethidium, S2/1 μg/ml ethidium, and S2/10 μg/ml of ethidium. Cells were incubated with ethidium for 30 min in Dulbecco's modified minimal essential medium at 37°C. The measurements were carried out in buffered Hank's balanced salt solution, in the presence of ethidium bromide with the same concentrations than those used for incubation.

experiment, digitonin is assumed to permeabilize the mitochondrial inner membrane, resulting in a collapse of the electrochemical gradient.

Anisotropy decay of ethidium fluorescence in the nucleus of living cells

The anisotropy decays, $r(t)$, of ethidium fluorescence, arising from a nuclear volume of a living cell, are shown in Fig.

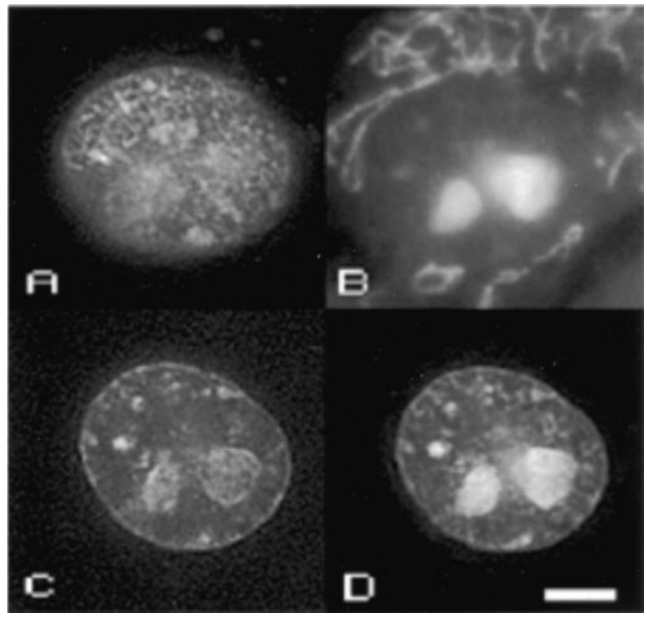

FIGURE 5 Relaxation of inhibition of ethidium intercalation in nuclear DNA of a living cell by digitonin treatment. Steady-state fluorescence image of an S2 cell (*A*, *B*) alive, and (*C*, *D*) after permeabilization by digitonin. (*A* and *C*) Hoechst 33342 fluorescence, $\lambda_{exc} = 365$ nm, OD = 2, and 480 nm $< \lambda_{em} <$ 520 nm. (*B* and *D*) Ethidium fluorescence, $\lambda_{exc} =$ 540 nm, OD = 2, and $\lambda_{em} >$ 590 nm. Bar 10 μm.

6 for three applied ethidium concentrations (0.4, 4, and 10 μg/ml). The anisotropy decay was calculated and plotted after corrections for normalization of $i_{vh}(t)$ and $i_{hh}(t)$ (Materials and Methods and Appendix A). The acquisition time was 45–60 min, during which the fluorescence intensity remained stable. In some cases, the fluorescence intensity increased, because the cell became apoptotic (data not shown) and the experimental data were discarded. The anisotropy decay curves are noisy at long relaxation time (70 ns), despite the length of the acquisition time, due to the very low level of fluorescence inside living cells. Two features could be revealed, however, from these data: 1) the relaxation of ethidium fluorescence anisotropy was very slow, and 2) the curves exhibit a dip-and-rise of anisotropy. Such dip-and-rise was previously reported on DNA or tRNA-ethidium sample in solution (Hazlett et al., 1989; Guest et al., 1991; Brochon, 1994) and constitutes the weighted mean anisotropy of two independent species, characterized by two different fluorescence lifetimes and two relaxation times,

$$r(t) = \frac{d_1(t)r_1(t) + d_2(t)r_2(t)}{d_1(t) + d_2(t)} \qquad (21)$$

where $d_i(t)$ is the fluorescence decay and $r_i(t)$ the anisotropy decay of the ith species (Knutson et al., 1986). The dip-and-rise of the anisotropy relaxation could be simulated by our model of decay-associated anisotropy, resting on the coexistence of two distinct ethidium species (50% each), one with short lifetime (1.8 ns) and short anisotropy relaxation time (250 ps), the other with long lifetime (22 ns) and long anisotropy relaxation time (250 ns), corresponding to free and intercalated ethidium, respectively. The simulation agreed with our experimental curves in Fig. 7. Thus, the dip-and-rise of ethidium fluorescence anisotropy indicates the presence of free ethidium in large proportion, whatever the total concentration, and further confirms that ethidium intercalation is prevented in nuclear DNA of living proliferating cells.

Restrained torsional dynamics of nuclear DNA in living cells

The ethidium fluorescence anisotropy decays in Fig. 6 had been obtained with ethidium present in the extracellular medium. To eliminate the contribution of free ethidium and to measure the pure fluorescence anisotropy decay of intercalated ethidium, the cells were rinsed. Lifetime measurements after rinsing confirmed that free ethidium was absent in the nucleus and that the amount of intercalated ethidium decreased only very slowly during the experiment: less than 5% of intercalated molecules were dissociated at the end (data not shown). Figure 8 *A* shows the anisotropy decay of nuclear ethidium fluorescence after rinsing: the dip-and-rise behavior was absent and a very slow fluorescence anisotropy relaxation remained. At higher ethidium concentration of 10 μg/ml, intercalated molecules had a similar fluorescence anisotropy (not shown).

As explained in the Discussion, RNA contribution was considered to be negligible. To estimate the degree of torsional restriction of nuclear DNA, we compared the anisotropy with that of a model system of naked DNA. The fluorescence anisotropy decay of ethidium, intercalated in λ-phage DNA (Fig. 8 *C*). was characterized by the known fluorescence relaxation of ethidium intercalated in naked DNA. The shape of this anisotropy decay curve is similar to

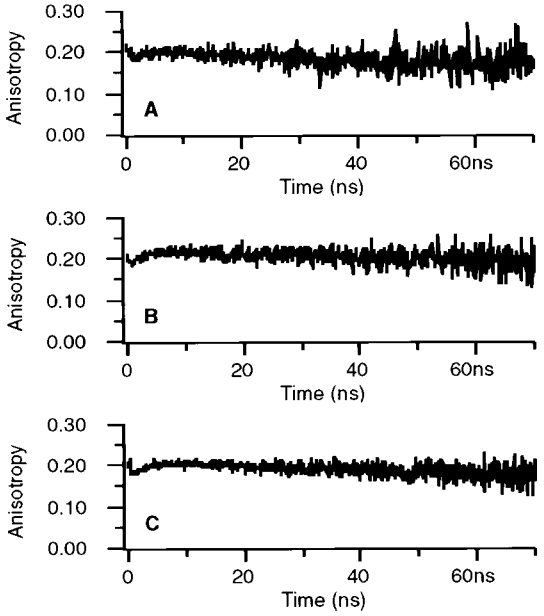

FIGURE 6 Anisotropy decays of nuclear ethidium fluorescence in a living cell. Different concentrations of ethidium bromide during incubation were used: (*A*) 1 μg/ml, (*B*) 4 μg/ml, (*C*) 10 μg/ml. Experiments were carried out in the presence of ethidium in the buffer. The fluorescence decays used for the calculation of the anisotropy function were normalized by the experimental method, using *G* and *T* factors.

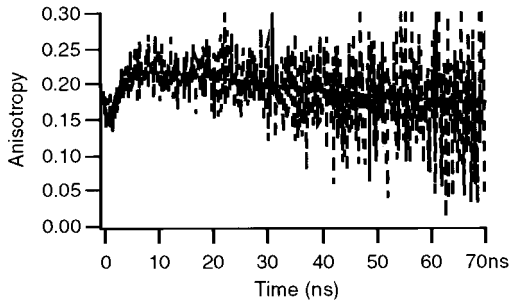

FIGURE 7 Simulation of dip-and-rise of anisotropy decay. Simulation is based on a model using two distinct species at the same concentration, one with short lifetime (1.8 ns) and short anisotropy relaxation time (250 ps), the other with long lifetime (22 ns) and long anisotropy relaxation time (250 ns).

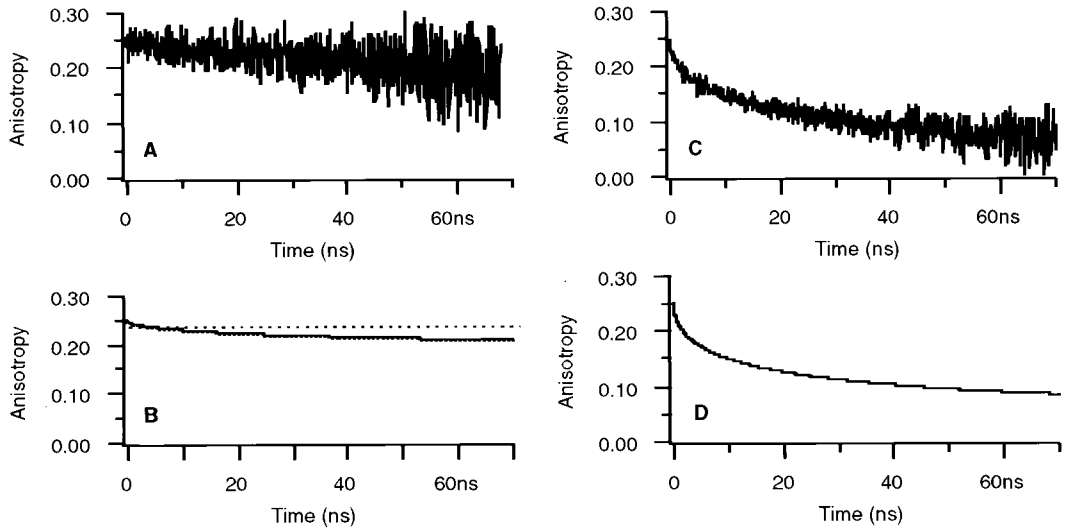

FIGURE 8 Anisotropy decays and simulations of intercalated ethidium fluorescence in the nucleus of a living S2 cell and in λ-phage DNA. (*A*) Nucleus in a living S2 cell, incubated in the presence of 4 μg/ml ethidium followed by rinsing. (*B*) Anisotropy relaxation simulation, using the model developed by Schurr (Schurr, 1984; Schurr and Schurr, 1985) with two sets of parameters: (*dotted*) $N = 20$, $\alpha = 6.5 \times 10^{-12}$ dyne · cm, and $\gamma = 6 \times 10^{-23}$ dyne · cm · s; (*solid*) $N = 100$, $\alpha = 6.5 \times 10^{-12}$ dyne · cm, and $\gamma = 6 \times 10^{-22}$ dyne · cm · s. (*C*) Solution of λ-phage DNA at 50 μg/ml in the presence of 4 μg/ml of ethidium bromide. (*D*) Simulation of anisotropy relaxation, using the model developed by Schurr and co-workers (Thomas et al., 1980) with $\alpha = 8 \times 10^{-12}$ dyne · cm and $\gamma = 1.4 \times 10^{-23}$ dyne · cm · s.

that obtained from simulation of torsional dynamics of naked DNA (Fig. 8 *D*), according to the model developed by Schurr (Thomas et al., 1980). For this simulation (Fig. 8 *D*), α (torsional coefficient) was 6.5×10^{-12} dyne·cm and γ (frictional coefficient) was 6×10^{-23} dyne·cm·s. These values of torsional dynamics parameters correspond to those given in the literature for naked DNA (Thomas et al., 1980; Heath et al., 1996).

In contrast, the fluorescence anisotropy of ethidium, intercalated in the nucleus of living cell relaxed more slowly (Fig. 8 *A*). Simulations of anisotropy decay were carried out using a model modified by Schurr and co-workers, where ethidium is intercalated in finite domains of basepairs rigidly clamped at both ends (Schurr, 1984; Schurr and Schurr, 1985) (see Materials and Methods). The bending motions were neglected. Three parameters, α, γ, and N, are now involved in this model, with N being the number of sequential basepairs involved in the torsional movements. The simulations evidenced that the torsional dynamics of the intercalating sites are restrained, either because N is low, or because γ is high (Fig. 8 *B*), corresponding either to short tracts of naked DNA that are clamped at both ends or to increased viscosity of the surrounding medium caused by protein interaction all along the domain. Further kinetic studies will be able to discriminate between these two hypotheses, which are of different biological significance.

At present, we do not have the proof that, in the nucleus of living cells, ethidium is exclusively intercalated in DNA and not also in RNA. If there was RNA contribution to the fluorescence, however, the inhibition of ethidium intercalation in nuclear DNA would be even stronger and, consequently, the DNA torsional dynamics further restrained (see below).

DISCUSSION

Time-correlated single-photon counting, adapted to confocal microscopy, allowed detection of molecules of ethidium, free (lifetime 1.8 ns) and intercalated (lifetime 22 ns), in the nuclear area of living cells that were incubated with this intercalating probe. Comparable concentrations of free ethidium were present in the nucleus and in the extracellular medium, demonstrating that the ethidium cation can diffuse within cytoplasm and nuclear area. Thus, the old hypothesis is no longer valid, according to which the absence, in living cells, of detectable steady-state ethidium fluorescence in the nucleus is due to impermeability of the cytoplasmic membrane. The ethidium cation gives rise to a strong fluorescence in mitochondria. Simultaneously, it is present as free molecules in the nucleus, thus ruling out the possibility that trapping in mitochondria would prevent interaction with nuclear DNA. The lack of ethidium fluorescence in the nucleus of living cells, as seen from steady-state measurements, is consequently due to reduced propensity of ethidium intercalation into chromatin DNA. This feature is characteristic of the living state in proliferating mammalian cells.

By taking advantage of the extreme sensitivity of time-correlated single-photon counting, as few as 100 molecules

of intercalated ethidium could be detected in a subnuclear volume of $\sim 1\ \mu m^3$. Moreover, fluorescence anisotropy decays from these few ethidium molecules could be obtained. The combination of fluorescence lifetime and fluorescence anisotropy dynamics reveals that the inhibition of ethidium intercalation in nuclear DNA is concomitant with restrained torsional DNA dynamics.

The nucleus of a living cell is a spatially organized organelle, composed of DNA, RNA, proteins, ions, water, and other molecules. The present thesis of restrained torsional dynamics of DNA in this organelle strongly rests on the following observations:

1. The inhibition of ethidium intercalation in nuclear DNA of living proliferative cells was evidenced by the very small amount of intercalated ethidium (identified by its 22-ns fluorescence lifetime) in the presence of free nuclear ethidium (1.8-ns fluorescence lifetime), even at higher ethidium concentrations. The above bi-exponential fluorescence decay is in strong contrast to the single-exponential fluorescence decay of 22 ns, observed in the case of naked DNA in solution. An independent confirmation for the existence of free ethidium in the nucleus was obtained from the dip-and-rise of fluorescence anisotropy, which was seen only, when free ethidium was present in the extracellular milieu and hence in the nucleus: the short component of the anisotropy decay in the presence of ethidium is that of freely rotating ethidium.
2. If the intercalation sites were concentrated within short nuclear DNA segments (see discussion below), energy homotransfer could not be ruled out, even at low ethidium concentrations. As discussed by others (Wu et al., 1991), homotransfer contributions would produce similar anisotropy decays at low ethidium/basepair ratios (up to 0.20 for naked DNA). At higher ratios, very rapid depolarization should occur, on a time scale too short to be resolved, under significant reduction of the initial anisotropy, r_0. Homotransfer could potentially explain, therefore, the lower r_0, found for fluorescence anisotropy of nuclear intercalated ethidium, compared with that of rhodamine 6G. Homotransfer, if present, would lead to an underestimation, however, of the torsional rigidity of DNA in the living cell, thus even enhancing our conclusions.
3. For each ethidium molecule intercalated, the DNA helix unwinds by 26° (Wang, 1974; Pulleyblank and Morgan, 1975). The mechanism of intercalation is controlled by Brownian structural fluctuations of DNA and not by a diffusive process (Sobell et al., 1976; MacGregor et al., 1987; Meyer-Almes and Porschke, 1993). The effective binding constant of ethidium intercalation and internal dynamics of DNA are correlated (Härd and Kearns, 1990; Clendenning et al., 1994; Heath et al., 1996). A decreased ethidium-binding constant occurs in parallel with restrained torsional motion in small circular plasmid (Heath et al., 1996), in DNA-transcriptional factor complexes (Härd and Kearns, 1990), and in nucleosome core particles (Winzeler and Small, 1991). In the unlikely event that all of the intercalated ethidium molecules were bound to RNA and not to DNA, the internal dynamics of nuclear DNA would have to be even more restrained, due to the absolute impossibility of ethidium intercalation in DNA. Thus, both the strong inhibition of intercalation and the extremely slow anisotropy relaxation for intercalated ethidium contribute to demonstrate that the torsional dynamics of nuclear DNA is globally restrained in the living state.

Intercalated ethidium could provoke the dissociation of proteins from nuclear DNA and the present experiments would not feature the unperturbed chromatin state in the living cell. Indeed, increasing ethidium concentrations were shown to release proteins from chromatin (Schröter et al., 1985) and to cooperatively release histones from DNA on isolated nucleosomes (McMurray and van Holde, 1991; Winzeler and Small, 1991). This behavior is in contrast to our low-concentration ethidium system: the ratio of free/intercalated ethidium in the nucleus did not vary significantly with increasing applied concentration of the cation, and the fluorescence anisotropy relaxations were superimposable for the different ethidium concentrations applied. These two facts strongly suggest that, under our minimal-invasive experimental conditions, DNA–protein interactions are not perturbed. Moreover, the internal dynamics of linear DNA is unaffected by ethidium, even at high degree of intercalation (Wu et al., 1991; Smith et al., 1992; Clendenning et al., 1994). Hence, the fluorescence anisotropy decay of intercalated ethidium, acquired under our conditions, is likely to probe the native state of chromatin.

We can deduce that the regions of nuclear DNA, where ethidium intercalates, represent segments of highly constrained torsional motion. The constrained state can originate from miscellaneous mechanisms, not mutually exclusive: i.e., secondary structural alterations by bending strain (Clendenning et al., 1994; Heath et al., 1996); specific protein interaction, wrapping around histone octamer in nucleosomal compaction (Winzeler and Small, 1991); and introduction of bent regions (Härd and Kearns, 1990).

A careful study of torsional motion of DNA in nucleosome core particles, using fluorescence anisotropy decays of intercalated ethidium (Winzeler and Small, 1991), revealed a highly constrained torsional motion of DNA, at low ethidium/basepair ratio, close to that in living cells of the present work ($\sim$0.0001 dye/basepair). In living proliferating cells, however, chromatin DNA exhibits different characteristics compared to DNA in a suspension of nucleosome core particles: at higher free ethidium concentrations, detected in the nucleus of living proliferating cells, the torsional dynamics of nuclear DNA remains highly constrained, whereas, in DNA of nucleosome core particle, the constraint is cooperatively released due to nucleosome dis-

sociation. Thus, the protein–DNA interactions inside nucleosomes in this type of living cells appear to be tighter than in isolated nucleosomes.

Packaging DNA templates in chromatin inhibits the progression of RNA and DNA polymerases in vitro (reviewed in Owen-Hughes and Workman, 1994; Widom 1998). Nevertheless, a living cell efficiently replicates and transcribes its nuclear DNA in vivo. In recent models, derived from in vitro analysis on polymerization over polynucleosomated templates, the existence of naked DNA regions was supposed to occur, transiently, over short segments (as short as 10 bp), due to partial or full dissociation of the histone octamer from the DNA (Studitsky et al., 1997). Intercalating molecules have been shown to interact in vitro mostly with internucleosomal linker regions of chromatin (Angerer and Moudrianakis, 1972; Sogo et al., 1984; McMurray and van Holde, 1991; Yao et al., 1993) or, to some extent, with kinks of DNA at the octamer surface (Hogan et al., 1987). Thus, the nuclear DNA intercalation sites of living cells could correspond to either internucleosomal regions ("linkers"), or to other DNA regions, being in interaction with specific proteins (replicating-transcribing complexes or other compounds, such as RNA).

A precise determination of the Schurr-model parameters (α, γ, and N), which would fit the torsional dynamics of DNA in vivo, is required for a better understanding of the origin of the constrained state: is it due to tightly closed clamped ends (small value of N corresponding to linkers) or to protein interaction involving an extended domain ($N >$ 100 bp and large values of α or γ)?

The inhibition of ethidium intercalation in the nucleus disappears after permeabilization, although the concentration of free ethidium in the nucleus does not change much. Permeabilization probably destroys the interactions of proteins or other biomolecules with DNA, as proposed earlier (Delic et al., 1991, 1992). Studies on DNA–protein interactions, carried out on extracted chromatin or on permeabilized cells, have to be interpreted with caution, therefore, and do not provide direct evidence for the structural state of native chromatin inside the living cell. Anisotropy decay studies provide a very helpful tool to probe the global internal dynamics of DNA, directly in living cells. Such anisotropy measurements, therefore, are extremely suitable to follow the dynamics of nuclear DNA in different contexts, such as proliferation or differentiation.

APPENDIX A: NORMALIZATION OF PARALLEL AND PERPENDICULAR FLUORESCENCE DECAYS FOR ANISOTROPY MEASUREMENTS IN EPIFLUORESCENCE MICROSCOPY

The optical design of the microscope results in four geometric components of the fluorescence polarization, where i_{vh} and i_{hv} pertain to the parallel direction and i_{vv} and i_{hh} to the perpendicular direction, relative to the direction of laser excitation. Parallel ($i_{vh}(t)$) and perpendicular ($i_{hh}(t)$) decays were acquired sequentially on the same sample spot. Although we discarded samples for which strong bleaching occurred during the acquisition of one of both decays, we cannot avoid weak bleaching and laser fluctuations. To correct for bleaching and fluctuations, the steady-state intensities for parallel and perpendicular orientation, i_{vh} and i_{hh}, were acquired immediately before starting the two decay acquisitions. The ratio of these steady-state intensities was used for normalization of the experimental decay curves $i_{vh}(t)$ and $i_{hh}(t)$, to obtain $i^N_{vh}(t)$ and $i^N_{hh}(t)$ by comparing the steady-state ratio with the ratio obtained from the integrated decay curves, $\int i_{vh}(t)\,dt$ and $\int i_{hh}(t)\,dt$, acquired within a 200-ns time window,

$$i^N_{vh}(t) = \left[i_{vh} \Big/ \int i_{vh}(t)\,dt \right] \times i_{vh}(t) \tag{A1}$$

and

$$i^N_{hh}(t) = \left[i_{hh} \Big/ \int i_{hh}(t)\,dt \right] \times i_{hh}(t) \tag{A2}$$

We define the correction factor, T, as

$$i^N_{vh}(t)/i^N_{hh}(t) = T \times i_{vh}(t)/i_{hh}(t), \tag{A3}$$

where

$$T = i_{vh} \times \int i_{hh}(t)\,d(t)/i_{hh} \times \int i_{vh}(t)\,d(t). \tag{A4}$$

A second correction was performed to take into account the different transmission efficiency of each geometric component of the excited and emitted polarized light, as well as depolarizing (or polarizing) effects linked to the microscope optics (objectives lenses, dichroic mirror). The actual parallel and perpendicular fluorescence intensities, i_{par} and i_{per}, are related to the experimental steady-state intensities by the following relations:

$$i_{vh} = S_v \times S'_h \times i_{par} \qquad i_{vv} = S_v \times S'_v \times i_{per} \tag{A5}$$

$$i_{hv} = S_h \times S'_v \times i_{par} \qquad i_{hh} = S_h \times S'_h \times i_{per}.$$

S_v and S_h are the transmission efficiencies, respectively, for vertical and horizontal polarization of the excitation light, and S'_v and S'_h are the transmission efficiencies, respectively, for the vertical and horizontal polarization of the emission. From expressions A5, it can be calculated that

$$i_{vh}/i_{hh} = [S_v/S_h] \times [i_{par}/i_{per}] \tag{A6}$$

and

$$(i_{vh} \times i_{vv})/(i_{hv} \times i_{hh}) = (S_v/S_h)^2. \tag{A7}$$

Combining Eqs. A6 and A7 gives

$$i_{vh}/i_{hh} = [(i_{vh} \times i_{vv})/(i_{hv} \times i_{hh})]^{1/2} \times i_{par}/i_{per}. \tag{A8}$$

For $i^N_{vh}(t)$ and $i^N_{hh}(t)$, the previously normalized time-dependent intensities, Eq. A8, become

$$i^N_{vh}(t)/i^N_{hh}(t) = G \times i_{par}(t)/i_{per}(t), \tag{A9}$$

where

$$G = [(i_{vh} \times i_{vv})/(i_{hv} \times i_{hh})]^{1/2}. \tag{A10}$$

Combining Eq. A3 and A9 gives

$$i_{par}(t)/i_{per}(t) = (T/G) \times (i_{vh}(t)/i_{hh}(t)). \quad \text{(A11)}$$

The anisotropy function $r(t)$ is defined by

$$r(t) = [i_{par}(t) - i_{per}(t)]/[i_{par}(t) + 2i_{per}(t)]. \quad \text{(A12)}$$

By combining Eq. A11 and A12, the value $r(t)$ is directly obtained from the experimental decays, $i_{vh}(t)$ and $i_{hh}(t)$, and from the T and G factors measured at each anisotropy experiment:

$$r(t) = [Ti_{vh}(t) - Gi_{hh}(t)]/[Ti_{vh}(t) + 2Gi_{hh}(t)]. \quad \text{(A13)}$$

APPENDIX B: FLUORESCENCE ANISOTROPY DECAY FOR FAST ROTATING CHROMOPHORES

For small molecules in solution, having a rotational time short with regard to the fluorescence lifetime, we can assume that, at long times after the laser pulse, all molecules are relaxed. The parallel and perpendicular polarized decays can then be normalized by the standard tail matching method. Only the determination of a correction factor, g, is required to take into account the different transmission light efficiencies of the two directions of polarization.

The anisotropy function $r(t)$ is defined by

$$r(t) = D(t)/S(t), \quad \text{(B1)}$$

where

$$D(t) = i_{par}(t) - i_{per}(t) \quad \text{(B2)}$$

is the difference between the parallel and the perpendicular decay, and

$$S(t) = i_{par}(t) + 2i_{per}(t) \quad \text{(B3)}$$

is the decay of total intensity. By combining Eq. B1, B2, and B3,

$$3i_{par}(t) = S(t) \times [1 + 2r(t)] \quad \text{(B4)}$$

and

$$3i_{per}(t) = S(t) \times [1 - r(t)]. \quad \text{(B5)}$$

For rhodamine 6G in butanol, $S(t)$ can be fitted with the theoretical model function,

$$S(t) = a/3 \times e^{-t/\tau}, \quad \text{(B6)}$$

with τ being the fluorescence lifetime and a being a constant. $r(t)$ can be fitted by the theoretical model function,

$$r(t) = r_0 e^{-t/\tau}, \quad \text{(B7)}$$

with r_0 being the anisotropy at time zero and ϕ the rotational time. It follows that

$$i_{par}(t) = ae^{-t/\tau} \times (1 + 2r_0 e^{-t/\phi}) \quad \text{(B8)}$$

and

$$i_{per}(t) = ae^{-t/\tau} \times (1 - r_0 e^{-t/\phi}). \quad \text{(B9)}$$

Two experimental fluorescence decays are acquired, $i_{vh}(t)$ and $i_{hh}(t)$, corresponding to the parallel and perpendicular polarized decay, respectively, for the microscope set-up used. These experimental decays are distorted by the measurement apparatus, and are related to the real time behavior, $i_{par}(t)$ and $i_{per}(t)$, by the convolution product of the instrument response function IRF(t),

$$i_{vh}(t) = \text{IRF}(t) * i_{par}(t) \quad \text{(B10)}$$

and

$$i_{hh}(t) = g \times \text{IRF}(t) * i_{per}(t), \quad \text{(B11)}$$

where g is the transmission correction factor. The two experimental decays were fitted using the expressions

$$i_{vh}(t) = \text{IRF}(t) * [ae^{-t/\tau} \times (1 + 2r_0 e^{-t/\phi})] \quad \text{(B12)}$$

and

$$i_{hh}(t) = g \times \text{IRF}(t) * [ae^{-t/\tau} \times (1 - r_0 e^{-t/\phi})]. \quad \text{(B13)}$$

This paper was supported by grants from Association pour la Recherche sur le Cancer, Physique et Chimie du Vivant, and European Union (#BIO4 CT97 2177). M.T. was supported by European Union fellowship.

REFERENCES

Allison, S. A., and J. M. Schurr. 1979. Torsion dynamics and depolarization of fluorescence of linear macromolecules. I. Theory and application to DNA. *Chem. Phys.* 41:35–59.

Ambroz, M., A. J. MacRobert, J. Morgan, G. Rumbles, M. S. C. Foley, and D. Philips. 1994. Time-resolved fluorescence spectroscopy and intracellular imaging of disulphonated aluminium phthalocyanine. *J. Photochem. Photobiol. B: Biol.* 22:105–117.

Angerer, L. M., and E. N. Moudrianakis. 1972. Interaction of ethidium bromide with whole and selectively deproteinized deoxynucleoproteins from calf thymus. *J. Mol. Biol.* 63:505–521.

Arents, G., and E. N. Moudrianakis. 1993. Topography of the histone octamer surface: repeating structural motifs utilized in the docking of nucleosomal DNA. *Proc. Natl. Acad. Sci. USA.* 90:10489–10493.

Ashraf, S. I., and Y. T. Ip. 1998. Transcriptional control: repression by local chromatin modification. *Curr. Biol.* 8:R683–R686.

Axelrod, D. 1979. Carbocyanine dye orientation in red cell membrane studied by microscopic fluorescence polarization. *Biophys. J.* 26: 557–574.

Axelrod, D. 1989. Fluorescence polarization microscopy. *Methods Cell Biol.* 30:333–352.

Baker, T. A., and S. P. Bell. 1998. Polymerases and replisome: machines within machines. *Cell.* 92:295–305.

Bastiaens, P. I. H., and A. Squire. 1999. Fluorescence lifetime imaging microscopy: spatial resolution of biochemical processes in the cell. *Trends Cell. Biol.* 9:48–60.

Beechem, J. M., E. Gratton, H. Hameloot, J. R. Knutson, and L. Brand. 1991. The global analysis of fluorescence intensity and anisotropy decay data: second generation theory and programs. *In* Topics in Fluorescence Spectroscopy: Principles. J. R. Lakowicz, editor. Plenum Press. New York. 241–305.

Brochon, J.-C. 1994. Maximum entropy method of data analysis in time-resolved spectroscopy. *Methods Enzymol.* 240:262–311.

Buurman, E. P., R. Sanders, A. Draauer, H. C. Gerritsen, J. J. F. van Deen, P. M. Houpt, and Y. K. Levine. 1992. Fluorescence lifetime imaging using a confocal laser scanning microscope. *Scanning.* 14:155–159.

Carey, M. 1998. The enhanceosome and transcriptional synergy. *Cell.* 92:5–8.

Clendenning, J. B., A. N. Naimushin, B. S. Fujimoto, D. W. Stewart, and J. M. Schurr. 1994. Effect of ethidium binding and superhelix density on the supercoiling free energy and torsion and bending constants of p30 delta DNA. *Biophys. Chem.* 52:191–218.

Coppey-Moisan, M., J. Delic, H. Magdelénat, and J. Coppey. 1994. Principle of digital imaging microscopy. *Methods Mol. Biol.* 33:359–393.

Coppey-Moisan, M., A.-C. Brunet, R. Morais, and J. Coppey. 1996. Dynamical change of mitochondrial DNA induced in the living cell by perturbing the electrochemical gradient. *Biophys. J.* 71:2319–2328.

Dayel, M. J., E. F. Hom, and A. S. Verkman. 1999. Diffusion of green fluorescent protein in the aqueous-phase lumen of endoplasmic reticulum. *Biophys. J.* 76:2843–2851.

Delic, J., J. Coppey, H. Magdelénat, and M. Coppey-Moisan. 1991. Impossibility of acridine orange intercalation in nuclear DNA of the living cell. *Exp. Cell Res.* 194:147–153.

Delic, J., J. Coppey, M. Ben Saada, H. Magdelénat, and M. Coppey-Moisan. 1992. Probing the nuclear DNA in living cell with fluorescent intercalating dyes. *J. Cell Pharmacol.* 3:126–131.

Durieux, C., A. C. Brunet, V. Geeraert, J. Coppey, and M. Coppey-Moisan. 1999. A transient decrease of electrochemical gradient stabilizes DNA structural change in single mitochondria of living cells. *Biol. Cell.* 91:597–604.

Echols, H. 1986. Multiple DNA–protein interactions governing high-precision DNA transactions. *Science.* 233:1050–1056.

Favard, C., J. Pager, D. Locker, and P. Vigny. 1997. Incorporation of ethidium bromide in the *Drosophila* salivary gland approached by microspectrofluorometry: evidence for the presence of both free and bound dye in the nuclei of cells in viable conditions. *Eur. Biophys. J.* 25:225–237.

French, T., E. Gratton, and J. Maier. 1992. Frequency domain imaging of thick tissues using a CCD. *SPIE Proc.* 1604:254–261.

Gadella, T. W. J. Jr., T. M. Jovin, and R. M. Clegg. 1993. Fluorescence lifetime imaging microscopy (FLIM): spatial resolution of microstructures on the nanosecond time scale. *Biophys. Chem.* 48:221–239.

Gao, M., and D. M. Knipe. 1989. Genetic evidence for multiple nuclear functions of the herpes simplex virus ICP8 DNA-binding protein. *J. Virol.* 63:5258–5267.

Grosschedl, R. 1995. Higher-order nucleoprotein complexes in transcription: analogies with site-specific recombination. *Curr. Opin. Cell Biol.* 7:362–370.

Guest, C. R., R. A. Hochstrasser, C. G. Dupuy, D. J. Allen, S. J. Benkovic, and D. P. Millar. 1991. Interaction of DNA with the Klenow fragment of DNA polymerase I studied by time-resolved fluorescence spectroscopy. *Biochemistry.* 30:8759–8770.

Härd, T., and D. R. Kearns. 1990. Reduced DNA flexibility in complexes with a type II DNA binding protein. *Biochemistry.* 29:959–965.

Hayashi, J.-I., M. Takemitsu, Y.-I. Goto, and I. Nonaka. 1994. Human mitochondria and mitochondrial genome function as a single dynamic cellular unit. *J. Cell Biol.* 125:43–50.

Hazlett, T. L., Johnson, A. E., and D. M. Jameson. 1989. Time-resolved fluorescence studies on the ternary complex formed between bacterial elongation factor Tu, guanosine 5′-triphosphate, and phenyalanyl-tRNA^{Phe}. *Biochemistry.* 28:4109–4117.

Heath, P. J., J. B. Clendenning, B. S. Fujimoto, and J. M. Schurr. 1996. Effect of bending strain on the torsion elastic constant of DNA. *J. Mol. Biol.* 260:718–730.

Hernandez, L. I., M. Zhong, S. H. Courtney, L. A. Marky, and N. R. Kallenbach. 1994. Equilibrium analysis of ethidium binding to DNA containing base mismatches and branches. *Biochemistry.* 33: 13140–13146.

Hogan, M. E., T. F. Rooney, and R. H. Austin. 1987. Evidence for kinks in DNA folding in the nucleosome. *Nature.* 328:554–557.

Jupe, E. R., R. R. Sinden, and I. L. Cartwright. 1993. Stably maintained microdomain of localized unrestrained supercoiling at a *Drosophila* heat shock gene locus. *EMBO J.* 12:1067–1075.

Knutson, J. R., L. Davenport, and L. Brand. 1986. Anisotropy decay associated fluorescence spectra and analysis of rotational heterogeneity. 1. Theory and applications. *Biochemistry.* 25:1805–1810.

Lakowicz, J. R., H. Szmacinski, K. Nowaczyk, K. W. Berndt, and M. Johnson. 1992. Fluorescence lifetime imaging. *Anal. Biochem.* 202: 316–330.

Lamond, A. I., and W. C. Earnshaw. 1998. Structure and function in the nucleus. *Science.* 280:547–553.

Leuba, S. H., C. Bustamante, J. Zlatanova, and K. van Holde. 1998. Contributions of linker histones and histone H3 to chromatin structure: scanning force microscopy studies on trypsinized fibers. *Biophys. J.* 74:2823–2829.

Luger, K., A. W. Mader, R. K. Richmond, D. F. Sargent, and T. J. Richmond. 1997. Crystal structure of the nucleosome core particle at 2.8 Å resolution. *Nature.* 389:251–260.

Macgregor, R. B. Jr., R. M. Clegg, and T. M. Jovin. 1987. Viscosity dependence of ethidium-DNA intercalation kinetics. *Biochemistry.* 26: 4008–4016.

Manders, E. M. M., H. Kimura, and P. R. Cook. 1999. Direct imaging of DNA in living cells reveals the dynamics of chromosome formation. *J. Cell Biol.* 144:813–821.

McMurray, C. T., and K. E. van Holde. 1991. Binding of ethidium to the nucleosome core particle. I. Binding and dissociation reactions. *Biochemistry.* 30:5631–5643.

Meyer-Almes, F. J., and D. Porschke. 1993. Mechanism of intercalation into the DNA double helix by ethidium. *Biochemistry.* 32:4246–4253.

Minami, T., and S. Hirayama. 1990. High quality fluorescence decay curves and lifetime imaging using an elliptical scan streak camera. *J. Photochem. Photobiol. A: Chemistry.* 53:11–21.

Morgan, C. G., A. C. Mitchell, and J. G. Murray. 1992. Prospects for confocal imaging based on nanosecond fluorescence decay time. *J. Microsc.* 165:49–60.

Nakatani, K., H. Misawa, K. Sasaki, N. Kitamura, and H. Masuhara. 1993. Pyrene excimer formation in individual oil droplets dispersed in gelatin matrices: space and time-resolved fluorescence spectroscopy. *J. Phys. Chem.* 97:1701–1706.

O'Connor, D. V., and D. Phillips. 1984. Time-Correlated Single Photon Counting. Academic Press. New York.

Olmsted, J. III, and D. R. Kearns. 1977. Mechanism of ethidium bromide fluorescence enhancement on binding to nucleic acids. *Biochemistry.* 16:3647–3654.

Owen-Hughes, T., and J. L. Workman. 1994. Experimental analysis of chromatin function in transcription control. *Crit. Rev. Eukaryot. Gene Expr.* 4:403–441.

Philips, L. A., S. P. Webb, and J. H. Clark. 1985. High-pressure studies of rotational reorientation dynamics: the role of dielectric friction. *J. Chem. Phys.* 83:5810–5821.

Piston, D. W., D. R. Sandison, and W. W. Webb. 1992. Time-resolved fluorescence imaging and background rejection by two-photon excitation in laser scanning microscopy. *SPIE Proc.* 1604:379–389.

Pulleyblank, D. E., and A. R. Morgan. 1975. The sense of naturally occurring superhelices and the unwinding angle of intercalated ethidium. *J. Mol. Biol.* 91:1–13.

Rydberg, B., W. R. Holley, I. S. Mian, and A. Chatterjee. 1998. Chromatin conformation in living cell: support for a zig-zag model of the 30 nm chromatin fiber. *J. Mol. Biol.* 284:71–84.

Schoutteten, L., P. Denjean, and R. B. Pansu. 1997. Characterization of a confocal microscope for time-resolved photon counting fluorescence. *J. Fluor.* 7:155–165.

Schröter, H., G. Maier, H. Ponstingl, and A. Nordheim. 1985. DNA intercalators induce specific release of HMG 14, HMG 17 and other DNA-binding proteins from chicken erythrocyte chromatin. *EMBO J.* 4:3867–3872.

Schurr, J. M. 1984. Rotational diffusion of deformable macromolecules with mean local cylindrical symmetry. *Chem. Phys.* 84:71–96.

Schurr, J. M., and R. L. Schurr. 1985. DNA motions in the nucleosome core particle: a reanalysis. *Biopolymers.* 24:1931–1940.

Selvin, P. R., B. A. Scalettar, J. P. Langmore, D. Axelrod, M. P. Klein, and J. E. Hearst. 1990. A polarized photobleaching study of chromatin reorientation in intact nuclei. *J. Mol. Biol.* 214:911–922.

Smith, S. B., L. Finzi, and C. Bustamante. 1992. Direct mechanical measurements of the elasticity of single DNA molecules by using magnetic beads. *Science.* 258:1122–1126.

So, P. T. C., T. French, W. M. Yu, K. M. Berland, C. Y. Dong, and E. Gratton. 1995. Time-resolved fluorescence microscopy using two-photon excitation. *Bioimaging.* 3:49–63.

Sobell, H. M., C. C. Tsai, S. G. Gilbert, S. C. Jain, and T. D. Sakore. 1976. Organization of DNA in chromatin. *Proc. Natl. Acad. Sci. USA.* 73: 3068–3072.

Sogo, J. M., P. J. Ness, R. M. Widmer, R. W. Parish, and T. Koller. 1984. Psoralen-crosslinking of DNA as a probe for the structure of active nucleolar chromatin. *J. Mol. Biol.* 178:897–919.

Studitsky, V. M., G. A. Kassavetis, E. P. Geiduschek, and G. Felsenfeld. 1997. Mechanism of transcription through the nucleosome by eukaryotic RNA polymerase. *Science.* 278:1960–1963.

Thomas, J. C., S. A. Allison, C. J. Appellof, and J. M. Schurr. 1980. Torsion dynamics and depolarization of fluorescence of linear macromolecules. II. Fluorescence polarization anisotropy measurements on a clean viral ϕ29 DNA. *Biophys. Chem.* 12:177–188.

van Holde, K. E. 1989. Chromatin. A. Rich, editor. Springer-Verlag, New York.

Verkman, A. S., M. Armijo, and K. Fushimi. 1991. Construction and evaluation of a frequency-domain epifluorescence microscope for lifetime and anisotropy decay measurements in subcellular domains. *Biophys. Chem.* 40:117–125.

Wahl, P., J. Paoletti, and J.-B. Le Pecq. 1970. Decay of fluorescence emission anisotropy of the ethidium bromide-DNA complex evidence for an internal motion in DNA. *Proc. Natl. Acad. Sci. USA.* 65:417–421.

Wang, J. C. 1974. The degree of unwinding of the DNA helix by ethidium. I. Titration of twisted PM2 DNA molecules in alkaline cesium chloride density gradients. *J. Mol. Biol.* 89:783–801.

Widom, J. 1998. Structure, dynamics, and function of chromatin in vitro. *Annu. Rev. Biophys. Biomol. Struct.* 27:285–327.

Winzeler, E. A., and E. W. Small. 1991. Fluorescence anisotropy decay of ethidium bound to nucleosome core particles. 2. The torsional motion of the DNA is highly constrained and sensitive to pH. *Biochemistry.* 30:5304–5313.

Wu, P. G., B. S. Fujimoto, L. Song, and J. M. Schurr. 1991. Effect of ethidium on the torsion constants of linear and supercoiled DNAs. *Biophys. Chem.* 41:217–236.

Yao, J., P. T. Lowary, and J. Widom. 1993. Twist constraints on linker DNA in the 30-nm chromatin fiber: implications for nucleosome phasing. *Proc. Natl. Acad. Sci. USA.* 90:9364–9368.